HHS Public Access

Author manuscript

Circ Res. Author manuscript; available in PMC 2017 January 08.

Published in final edited form as:

Circ Res. 2016 January 8; 118(1): 56–72. doi:10.1161/CIRCRESAHA.115.306874.

Bioengineering Human Myocardium on Native Extracellular Matrix

Jacques P. Guyette[1,2], **Jonathan M Charest**[1], **Robert W Mills**[3], **Bernhard J. Jank**[1,2], **Philipp T. Moser**[1,2], **Sarah E. Gilpin**[1,2], **Joshua R. Gershlak**[4], **Tatsuya Okamoto**[1], **Gabriel Gonzalez**[1,2], **David J. Milan**[3,5], **Glenn R. Gaudette**[4], and **Harald C. Ott**[1,2,6,7]

[1]Center for Regenerative Medicine, Massachusetts General Hospital

[2]Harvard Medical School

[3]Cardiovascular Research Center, Massachusetts General Hospital

[4]Department of Biomedical Engineering, Worcester Polytechnic Institute

[5]Division of Cardiology, Massachusetts General Hospital

[6]Division of Thoracic Surgery, Department of Surgery, Massachusetts General Hospital

[7]Harvard Stem Cell Institute

Abstract

Rationale—More than 25 million individuals suffer from heart failure worldwide, with nearly 4,000 patients currently awaiting heart transplantation in the United States. Donor organ shortage and allograft rejection remain major limitations with only about 2,500 hearts transplanted each year. As a theoretical alternative to allotransplantation, patient-derived bioartificial myocardium could provide functional support and ultimately impact the treatment of heart failure.

Objective—The objective of this study is to translate previous work to human scale and clinically relevant cells, for the bioengineering of functional myocardial tissue based on the combination of human cardiac matrix and human iPS-derived cardiac myocytes.

Methods and Results—To provide a clinically relevant tissue scaffold, we translated perfusion-decellularization to human scale and obtained biocompatible human acellular cardiac scaffolds with preserved extracellular matrix composition, architecture, and perfusable coronary vasculature. We then repopulated this native human cardiac matrix with cardiac myocytes derived from non-transgenic human induced pluripotent stem cells (iPSCs) and generated tissues of increasing three-dimensional complexity. We maintained such cardiac tissue constructs in culture for 120 days to demonstrate definitive sarcomeric structure, cell and matrix deformation, contractile force, and electrical conduction. To show that functional myocardial tissue of human scale can be built on this platform, we then partially recellularized human whole heart scaffolds

Address correspondence to: Dr. Harald C. Ott, Assistant Professor in Surgery, Harvard Medical School, Division of Thoracic Surgery, Department of Surgery, Massachusetts General Hospital, 55 Fruit Street, Blake 15, Boston, MA 02114, hott@partners.org.

DISCLOSURES

HC Ott is founder and stockholder of IVIVA Medical Inc. This relationship did not affect the content or conclusions contained in this manuscript.

with human iPSC-derived cardiac myocytes. Under biomimetic culture, the seeded constructs developed force-generating human myocardial tissue, showed electrical conductivity, left ventricular pressure development, and metabolic function.

Conclusions—Native cardiac extracellular matrix scaffolds maintain matrix components and structure to support the seeding and engraftment of human iPS-derived cardiac myocytes, and enable the bioengineering of functional human myocardial-like tissue of multiple complexities.

Keywords

Pressure-controlled perfusion decellularization; iPS-derived cardiac myocytes; human myocardial tissue; extracellular matrix; cardiac regeneration; stem cell; cardiac differentiation

INTRODUCTION

More than 5 million people in the United States live with heart failure (HF), with more than 800,000 new cases diagnosed each year[1]. Patients suffer from poor quality of life, and require frequent interventions, leading to greater than 1 million hospital discharges and a cost of more than $39 billion per year[2]. While artificial mechanical support can be offered to a small group of patients, heart transplantation remains the only curative treatment option for end-stage HF. Donor organ shortage is its major limitation, as nearly 1,500 heart transplant candidates will endure extended waitlist periods while facing 5-year mortality rates of approximately 50%[2, 3]. While heart transplant recipients benefit from significantly improved short-term survival rates, long-term survival remains limited due to chronic rejection and adverse effects from lifelong immunosuppression[4]. The engineering of bioartificial myocardium, and ultimately of bioartificial hearts, from patient-derived cells could theoretically solve both of these problems. While many hurdles remain, the creation of bioartificial functional human myocardium from adult-derived, genetically non-altered cells is the first vertical step towards this goal, and can provide new pathways for repair and replacement of myocardium in HF patients.

The onset of HF is preceded by myocardial necrosis, fibrosis, and extracellular matrix (ECM) remodeling, resulting in progressive loss of architecture and contractile function[1, 2, 5]. Partial reverse remodeling and myocardial augmentation has been accomplished by direct delivery of contractile cardiac myocytes and passive biomaterials[6–9]. Following similar principles, different scaffold materials and cells have been combined to generate tissue-engineered myocardium. In both approaches contractile graft thickness is limited due to poor diffusion and neovascularization that fails to meet the demand of cardiac myocyte metabolism[10–12]. Graft architecture and electromechanical integration are constrained by non-physiologic scaffold properties, and the altered properties of scarred myocardium. Successful clinical application of myocardial regeneration will depend on the ability to establish physiologic tissue architecture, and immediate graft perfusion upon implantation. Native human heart matrix provides the physiologic micro and macro architecture, ECM composition, and the perfusable hierarchical vascular bed, serving as a foundational scaffold to engineer bioartificial myocardium[13, 14].

By translating our previous work to human scale[15], we demonstrate successful application of whole-organ perfusion decellularization to human hearts, and generate acellular cardiac scaffolds with preserved ECM material properties, structure, patent coronary conduits, with an immunologic profile that induces a constructive remodeling response. By comparing brain death and donation after cardiac death donors, we validate this new regenerative platform from more than 5,500 currently unused donor hearts per year[3]. By deriving cardiac myocytes from non-transgenic adult derived iPSC at clinical scale, we provide the necessary building blocks for clinically relevant myocardial regeneration. By repopulating native human heart matrix in sections, fibers, and biomimetic whole organ culture, we show the potential for creating functional human myocardial-like tissue from an autologous source to augment or replace lost myocardial function, and serve as a patient-specific development platform.

METHODS

All methods and associated references are included in the online data supplement.

RESULTS

Perfusion decellularization of human cadaveric hearts

In a first set of experiments, we scaled perfusion decellularization to donated human hearts that were recovered by the New England Organ Bank and deemed unusable for clinical transplantation. Between 2012 and 2015, 73human non-transplantable hearts were recovered for research after specific consent was obtained. Donor records (n = 73; 5 patient records unavailable) indicate a distribution of 36 males versus 32 females, 29 cardiac death donors (DCD) versus 39 brain death donors (DBD), an average age of 52.43 ± 14.29 years, an average height of 170.96 ± 9.53 cm, an average weight of 81.54 ± 20.53 kg, and an average body mass index of 27.76 ± 6.09 kg/m^2. Heart identification numbers, corresponding donor data, and associated experimental tests are outlined in Supplemental Table I. We applied aseptic pressure-controlled antegrade coronary flow to 40 hearts in a custom organ chamber (60 mm Hg, average cold ischemia time of 455 ± 184 minutes; Supplemental Fig. I). Hearts were perfusion-decellularized with 1% SDS (168 hrs), deionized H_2O (24 hrs), 1% Triton-X100 (24 hrs), and PBS washes (168 hrs) following a standardized protocol (Fig. 1A)[16]. Decellularized hearts contained 346.17 ± 27.92 ng/mg wet tissue of residual double-stranded DNA (dsDNA), which could be removed by treatment with endonuclease (Fig. 1B). Subsequent perfusion of decellularized whole-hearts with 25 U/mL of endonuclease at room temperature for 24 hrs demonstrated a 99.05% reduction in dsDNA (3.27 ± 3.12 ng/mg wet tissue, $p < 0.05$), with thresholds meeting established criteria for decellularized biomaterials[17]. Biochemical analysis of perfusion-decellularized hearts from both DCD and DBD donors indicated a high retention of insoluble collagen, moderate decrease of sulfated-glycosaminoglycans, and lower concentrations of α-elastin and soluble collagen (Fig. 1C, Supplemental Fig. II). Importantly, we did not detect measureable amounts of residual SDS in decellularized hearts (< 0.02% w/v extract; below detection limit)[18].

Proteomics analysis indicated an 89.14% reduction of the cadaveric cardiac proteome (967 proteins), with the identification of 105 unique proteins in decellularized hearts (Fig. 1D).

Matrisome proteins were identified by querying our cadaveric and decellularized lists of unique proteins with the UniProt database for the subcellular location search terms "extracellular matrix" and "basement membrane", exclusively and combined, as defined cellular component terms by the Gene Ontology Consortium[19, 20]. Acellular heart scaffolds showed a marked retention of 36 matrisome proteins following the perfusion decellularization process (Fig. 1D). Normalized relative abundances of uniquely identified matrisomal proteins in both cadaveric and decellularized human myocardium were further categorized into ECM-protein families (Fig. 1E). The four largest ECM-protein families are conserved across cadaveric and decellularized cardiac matrix (collagens, laminins, fibrillins, and proteoglycans), with the largest relative contributions to the decellularized scaffolds being fibrillin-1, collagen IV, heparin sulfate, and laminin gamma-1. Whole lists of unique proteins for both cadaveric and decellularized myocardium are provided (Supplemental Tables II, III). Histological evaluation confirmed the retention of collagens (I, III, and IV), laminin, and fibronectin within acellular human heart scaffolds (Fig. 1F, Supplemental Fig. III). Cardiac matrix fiber composition and architecture were maintained, showing vacant spacing between fibers with a loss of nuclei and the cardiac myocyte marker myosin heavy chain. Insoluble adipose tissue matrix and lipid molecules remain on the epicardial surface after decellularization (Fig. 1A), but further histological analysis confirmed the absence of cells and preservation of matrix structure (Supplemental Fig. IV). In evaluation of how the decellularization process affects the material properties of the cardiac matrix scaffold, equibiaxial mechanical testing of transmural samples displayed similar moduli between cadaveric and decellularized samples, along both the base/apex axis (376.3 ± 191.7 vs. 370.8 ± 150.9 kPa) and the septum/free-wall axis (581.4 ± 325.5 vs. 451.4 ± 257.8 kPa; Fig. 1G). Anisotropic elastic behavior was measured by an "anisotropy ratio" comparing the difference and the sum of the two orthogonal moduli within a tissue sample. A value of zero indicates perfect biaxial isotropy while a value approaching one indicates a high degree of anisotropy. Cadaveric and decellularized samples exhibited measurable anisotropic ratios (0.314 ± 0.196 and 0.167 ± 0.158; Fig. 1H) that were statistically different from zero (p = 0.0027 and p = 0.0086), but not statistically different from each other (p = 0.0984).

Immunogenic profile of decellularized human cardiac matrix

Taking a critical step towards the potential use of our human cardiac scaffolds in clinical applications, we assessed the immunogenic profile of perfusion-decellularized myocardium after subcutaneous implantation in Sprague-Dawley rats for two weeks. Comparisons were made versus cadaveric human myocardium, as well as decellularized porcine myocardium that was perfusion-decellularized in the same manner as donated human hearts described above[16]. Histological evaluation of explanted material by immunofluorescence showed a considerable number of CD68+ mononuclear cells in all three groups. There appeared to be a more discernable M1-macrophage proinflammatory response by cadaveric human and decellularized porcine myocardium, while decellularized human myocardium presented with a more definitive M2-macrophage immunomodulatory response (Fig. 2A). A CellProfiler image processing pipeline and CellProfiler Analyst were used to quantify macrophage phenotype across images (Supplemental Fig. V)[21, 22]. From all cells counted in each high-power field (number of fields/group: 28 ± 1; number of cells/field: 1,152.5 ± 294.2), cadaveric human tissue contained 70.49 ± 1.72% CD68+ cells, while decellularized human

matrix contained 79.63 ± 3.22%, and decellularized porcine matrix contained 66.44 ± 6.17% CD68+ cells (Fig. 2B). Co-staining with CD80 demonstrated the presence of M1 macrophage phenotype in cadaveric human tissue (63.13 ± 9.79%), decellularized human matrix (52.11 ± 7.05%), and decellularized porcine matrix (67.73 ± 3.01%) from all cells counted per field. Co-staining for CD163 on adjacent sections revealed that cadaveric tissue implants elicited only 38.30 ± 7.46% M2+ cells, while decellularized human matrix implants elicited 69.54 ± 8.44% and decellularized porcine matrix elicited 53.52 ± 6.80% M2+ immunomodulatory cells ($p < 0.01$). A CD163/M2+ macrophage response has previously been shown as an indication of reconstructive remodeling described in decellularized matrices[23]. During tissue explantation at the 2-week time point, blood samples were also collected to analyze whole blood and serum. Whole blood analysis did not indicate a statistical difference between any groups with respect to total white blood cell components (Supplemental Fig. VI). Sera were also tested against human leukocyte antigen (HLA) single antigen beads, where experimental groups were normalized to the sham group, and antibody reactivity to beads with specific HLA alleles was determined by mean fluorescence intensity (MFI) using HLA Fusion software (version 3.0; One Lambda). Implanted decellularized human matrix showed reactivity to only 2 HLA beads, yielding values of <100 MFI that are well below the positive cut-off value of 500 MFI (Fig. 2C). Implanted cadaveric myocardium showed reactivity to >50 HLA beads, yielding values that ranged between 5000 and 7900 MFI, and showing high reactivity against patient-specific HLA types attributed to the implanted cadaveric myocardium (Fig. 2C). The single antigen bead assay confirmed our qualitative assessment (by immunofluorescence) that the decellularization process removes HLA from the cardiac matrix as cells are removed (Fig. 2D).

Decellularized coronary vasculature

In assessment of acellular coronary vasculature, DCD hearts had slightly lower coronary flow (Fig. 3A) and higher vascular resistance (Fig. 3B) compared to DBD hearts during detergent perfusion, but achieved similar flow and resistance by the end PBS washes. This initial difference did not reach statistical significance. Histological evaluation by pentachrome stain showed decellularized vasculature retained structural blood vessel features, with preservation of the intima, media, adventitia, and elastic laminas (Fig. 3C). Scanning electron microscopy further confirmed that the decellularization process removed all endothelial cells, without evidence of basement membrane disruption (Fig. 3D,E). Cardiac computed tomography scans revealed conservation of the conductance arteries of the coronary tree, showing structure and patent lumens stemming from the left and right main coronaries (Fig. 3F). Angiography of acellular hearts from patients presenting with coronary artery disease confirmed the preservation of perfusable coronary vessels, but revealed that the decellularization process does not resolve luminal narrowing related to atherosclerotic plaques (Supplemental Fig. VII). To visualize perfusion of microvasculature within decellularized hearts, we cannulated and directly perfused epicardial conductance arteries with resuspended 0.2 μm-diameter fluorescent microspheres, and tracked microsphere movement through mid-myocardial and endocardial regions using micro-optical coherence tomography (μOCT). Using a Z-projection tool to generate a running

average from the acquired video sequences, we confirmed bead-flow through distinct pathways or microvascular channels (Supplemental Video I).

To evaluate the preservation of microvasculature, we perfused cadaveric human hearts and decellularized human hearts with radio-opaque silicone, and performed a systematic comparison of full-thickness left ventricular samples by micro-computed tomography (μCT). Reconstructions of high-resolution μCT images were made on full-thickness samples from the epicardial surface to the endocardium, revealing that the decellularized cardiac matrix retains an intact vascular hierarchy, with branching extensions with diameters on the order of ~10 μm (Fig. 3G). Analyzing two-dimensional μCT images from the epi-, mid-, and endocardial regions for the number of vessels normalized to tissue area found similar vessel densities and trends between the cadaveric and decellularized hearts (Fig. 3H). In the subepicardial region, no statistical difference in vascular density was found between cadaveric myocardium (15.94 ± 3.03 vessels/mm^2) and decellularized matrix (13.44 ± 1.38). Likewise, both mid-myocardial and subendocardial regions showed no statistical difference in vascular densities between cadaveric myocardium (25.93 ± 0.40 and 20.64 ± 3.52, respectively) and decellularized matrix (22.44 ± 2.04 and 18.30 ± 3.6, respectively). Further analysis of the μCT images was done to measure the minor axis of vessel cross-sections as an indication of vessel diameter, which confirmed similar vessel-diameter distribution between the cadaveric and decellularized samples in all three myocardial sub-regions (Fig. 3I,J).

In vitro cardiac differentiation of BJ RiPS

To examine the translational value of our approach, we sought to generate a clinically relevant number of human cardiac myocytes from a non-transgenic cell source. We therefore obtained and expanded human BJ fibroblast RNA-induced pluripotent stem cells (BJ RiPS, clone 1.1)[24]. To induce cardiac differentiation, we applied temporal modulation of canonical Wnt/β-catenin signaling to BJ RiPS cultured in monolayer[25]. We then mapped gene expression profiles of 15 markers by RT-PCR at different developmental stages (days 0, 3, 5, 7, 14, 30, 60, 120, and 180) to monitor and define the profile of BJ RiPS through stages of cardiac differentiation and maintenance, and to define checkpoints for quality control required at a clinically relevant scale (Fig. 4A). Prior to the onset of differentiation at day 0, BJ RiPS exhibited definitive expression of classic pluripotency genes OCT4, SOX2, and NANOG. Treatment with Gsk3 inhibitor CHIR99021 for 24 hours markedly decreased OCT4, SOX2, and NANOG expression by day 3, while expression of genes typically found in mesendoderm and mesodermal tissues were elicited (MIXL1, T, ISL1, and GATA4). Starting on day 3, 48-hour treatment with Wnt inhibitor IWP4 decreased MIXL1, T, and ISL1 by day 5, while essential early-stage cardiac genes emerged (GATA4, NKX2.5, MEF2C, and TBX5). By day 7 through day 14 in cardiac maintenance media, definitive late-stage cardiac genes became expressed (MYH6, MYH7, MYL2, and TNNT2), as large areas of differentiated cardiac myocytes began spontaneously contracting by day 14 (Supplemental Video II). Early- and late-stage cardiac markers tended to increase by day 30, and expression persisted through days 60, 120, and 180 post-differentiation. By day 180, most cardiac genes appeared to taper, which is consistent with observations of decreased contractility within culture plates. In conjunction with increased cardiac gene expression, BJ

RiPS-derived cardiac myocytes isolated between days 30 and 60 post-differentiation showed positive cardiac protein expression and structure for sarcomeric α-actinin, cardiac troponin T, and myosin heavy chain by immunofluorescence (Fig. 4B). Cardiac protein expression in day 30–60 cardiac myocytes was further confirmed by flow cytometry, yielding high populations positive for sarcomeric α-actinin and cardiac troponin T (Fig. 4C), achieving differentiation efficiencies of >85%. As day 30–60 cardiac myocytes appeared to be most robust for cardiac gene and protein expression, cells within this time frame were enzymatically dispersed and isolated for seeding experiments.

Recellularization of myocardial slices and fibers

To test whether perfusion-decellularized human cardiac matrix can support engraftment of cardiac myocytes and enable myocardial tissue formation, we reseeded matrix sections (200 μm) with human iPS-derived cardiac myocytes in non-perfused two-dimensional culture (Fig. 5A). Acellular human heart matrix (Fig. 5Ai) supported the attachment, viability, and function of human cardiac myocytes (Fig. 5Aii) by evidence of spontaneously contracting slices within 4–7 days of culture. Serving as an early milestone for creating force-generating cardiac tissue, functional myocardial slices were robust and could be maintained for 120 days in culture. To characterize the mechanical function, we first used high spatial-resolution imaging (high density mapping, HDM)[26] to determine the area deformation of small defined regions of interest (Supplemental Fig. VIII). By independently analyzing matrix-seeded cardiac myocytes, as well as the underlying cardiac ECM within the same region (20 μm below the slice surface), we confirmed stable cell-matrix interaction and quantified the degree to which cell contractility translated to matrix deformation. In spontaneously contracting slices, cardiac myocytes achieved 0.59 ± 0.26% area strain at a natural frequency of 1.36 ± 0.32 Hz, which translated to 0.47 ± 0.17% area strain of the ECM with an average natural frequency of 1.38 ± 0.43 Hz (Fig. 5B). Functional myocardial slices could be electrically paced at 1 Hz or 2 Hz, and data for both cells and matrix could be captured at consistent dominant frequencies (Fig. 5B). Area strain of myocardial matrix could be significantly increased to 1.55 ± 0.55% when paced at 1 Hz, and decreased to 1.02 ± 0.31% when paced at 2 Hz. The technique to measure in vitro area strain is concurrent with the in vivo regional cardiac functional metric of systolic area contraction[27]. Regenerated human myocardial slices achieved strain below normal adult myocardium (~20%), however, the integration of human cardiac myocytes with human heart matrix formed mechanically active tissue on the same order of magnitude as compliant ECM cardiac patches tested in vivo (~4%)[27].

Moving to a more physiologic three-dimensional model, we reseeded non-perfused cardiac fibers (15 mm length, 2.5 mm diameter) cut from the left ventricular free wall of decellularized cardiac scaffolds (Fig. 5C). Reseeded cardiac fibers supported the attachment, viability, and function of human cardiac myocytes by evidence of spontaneously contracting tissue within 7–10 days, which could be maintained for 60+ days in culture (Supplemental Video III). Using micro-optical coherence tomography (μOCT) that allows for imaging contractility 250 μm within cardiac fibers with high spatial and temporal resolution (Fig 5C, Supplemental Video IV)[28], we then applied HDM and post-processing analysis for strain

analysis. Areas 100–200 μm within spontaneously contracting cardiac fibers achieved 8.32 ± 0.74% strain (Fig. 5D) at a frequency of 1.49 ± 0.06 Hz (Fig. 5E).

We measured force generation on myocardial slices by measuring deflections of contractile nodes using a custom setup for adhered slices (Supplemental Fig. IX,A). Force could be measured in spontaneously contracting cardiac tissues, and was modulated by electrical pacing (Fig. 5F). Spontaneously beating areas within unstimulated slices generated 14.93±3.85 μN of contractile force, which was decreased to 10.30 ± 2.81 μN when electrically stimulated at 2 Hz. Force generation in human myocardial slices was orders of magnitude higher than single human iPS-derived cardiac myocytes[29, 30], achieving 33.8% of native murine embryonic heart tissue (53.0±15.5 μN)[31], suggesting multicellular contractile tissue formation.

Using a more traditional setup to measure contractile force in muscle tissue (Supplemental Fig. IX,B), spontaneously contracting cardiac fibers generated 102.7 ± 76.3 μN of force, while electrical pacing at 2 Hz could increase force generation to 124.1 ± 94.7 μN (Fig. 5G) by recruiting more recellularized areas to contract in synchrony as a syncytium. Force curves measured from both myocardial slices and cardiac fibers were further analyzed to assess amplitude, period, time to 50% relaxation (TTR_{50}), and time to 90% relaxation (TTR_{90}) under different pacing conditions (Fig. 5H, Supplemental Fig. X). Cardiac fibers generated contractile force at an order of magnitude higher than myocardial slices, while decreasing trends for period, TTR_{50}, and TTR_{90} were similar for both constructs (Fig. 5H). Captured frequencies of both slices and fibers effectively correlated with pacing frequencies (Supplemental Fig. XI). Loading fiber-seeded cardiac myocytes with voltage-sensitive di-8-ANEPPS dye, cardiac fibers were tested in a custom pacing and imaging chamber to perform voltage mapping of cardiac electrical activity. Fibers paced with 10 V at 1 Hz generated electrical conductivity that could be mapped across large surface-areas, with a conduction velocity of 32 ± 56 cm/s (Fig. 5I). Action potentials at multiple points within conduction areas were assessed based on relative fluorescence intensity signal, with an average action potential duration at 80% (APD80) of 405 ± 116 ms. Immunofluorescent staining of reseeded fibers for cardiac markers sarcomeric α-actinin, cardiac troponin T, and myosin heavy chain showed large areas of cardiac myocytes with a striated phenotype, and a high degree of alignment (Fig. 5J). Further analysis by transmission electron microscopy (TEM) confirmed cardiac myocyte elongation and myocardial tissue formation, demonstrated by aligned myofibrillogenesis (Fig. 5K, left panel) and definitive sarcomeric structures (right panel).

Whole-heart experiments

Whole-heart recellularization experiments were carried out using a custom human heart bioreactor capable of providing coronary perfusion and LV wall mechanical stimulation (Fig. 6A). Mechanical stimulation was achieved by oscillating the pressure inside a balloon placed within the LV to determined targets, thus imparting strain to the LV wall (Fig. 6B). Validation of strain delivery with oscillating balloon pressure was performed using HDM on the presumed reseeding area of the LV wall of a decellularized porcine heart under mechanical stimulation in our bioreactor (Fig. 6C, Supplemental Video V).

We reseeded whole acellular human hearts with ~500 million human BJ RiPS-derived cardiac myocytes by making 5 intramyocardial injections into the basal anterior and mid anterior segments of the left ventricle (using ~500 μL/injection, for total volume of 2.5 mLs), between the left anterior descending and left circumflex coronary arteries (Fig. 6D). To improve cell retention, we adopted a technique in which mattress sutures were tied at each injection point before needle extraction to minimize cell loss (Fig. 6E)[32]. LV balloons were implanted through the mitral valve post cell delivery to prevent balloon puncture, and then pre-filled to fully occupy the ventricular cavity. Recellularized human hearts were then mounted in the human heart bioreactor to provide antegrade perfusion to the main coronary arteries and cultured for 14 days, with matrix strain stimulation starting on day 7 of culture (Fig. 6F, Supplemental Video VI).

Metabolic function was monitored during culture by sampling perfusate from the coronary sinus to compare against baseline media (Table 1). Over consecutive 48-hour culture periods for 10 days, no significant differences were found for measures of pH, pO_2, pCO_2, HCO_3, TCO_2, or percent O_2 saturation. However, a significant decrease of glucose suggested consumption (baseline: 186.33 ± 1.53 mg/dL, culture: 155.75 ± 6.70 mg/dL, $p < 0.01$). Conversely, significant lactate production was detected (baseline: 0 mmol/L, culture: 2.44 ± 0.19 mmol/L, $p < 0.01$).

After 14 days in culture, we performed electromechanical functional analysis on the regenerated myocardium, using a bench-top perfusion setup. Electrical stimulation was delivered through cardiac leads placed within the anterolateral wall of the left ventricle (0.8 Hz, 10–80 V, 5 ms). Stimulated myocardium generated visible contractions (Supplemental Video VII), with recordable repolarizations (Fig. 7A). Using a force transducer to measure force based on deflections of contracting regions on the epicardial surface, continuous electrical stimulation at 0.8 Hz could generate regional contractions measuring ~350 μN (Fig. 7B). By introducing a pressure transducer into the LV balloon and pre-filling the balloon to an isovolumetric pressure of 20 mmHg, stimulated myocardial contractions generated developed pressures of 2.4 ± 0.1 mmHg, with a dP/dt max of 139.7 ± 5.7 mmHg/s, a dP/dt min of 41.6 ± 3.5 mmHg/s, and a calculated tau of 47.3 ± 10.6 ms (Fig. 7C). Using an 8x8-pin plaque electrode array with pins spaced 2.54 mm apart, spontaneous depolarizations could be detected across the recellularized myocardium with action potential durations of 322 ms (Fig. 7D).

Histological analysis revealed dense regions of engrafted iPS-derived cardiac myocytes in the depth of the left ventricular wall, indicated by large areas of myosin heavy chain (MHC) positive cells in successive sections throughout recellularized volumes (Fig. 7E). By linear interpolation of the areas of MHC-positive signal in tissue sections across reseeded regions, we detected a tissue repopulation of up to 50% within the target region of 5 cm^3 (Fig. 7F, Supplemental Table I). Coronary perfusion during whole heart culture provided sufficient nutrient and oxygen supply to maintain >90% viability after 14 days in culture (Fig. 7G). Trichrome staining of recellularized areas confirmed engraftment, with reseeded cells integrating with cardiac matrix (Fig. 7H). Recellularized regions of whole-heart scaffolds contained large areas of cardiac myocytes that expressed sarcomeric α-actinin, cardiac troponin T, and myosin heavy chain by immunofluorescence (Fig. 7I). Reseeded cardiac

myocytes within biomimetically stimulated hearts appeared to demonstrate a range of maturity, where some cardiac myocytes showed rounded immature sarcomere formation, while other cardiac myocytes displayed elongated and striated phenotypes.

DISCUSSION

Loss of viable myocardium leads to architectural and functional decline, and ultimately results in the development of heart failure. Bioengineered myocardium generated from patient derived cells could provide an alternative to allo-transplantation and mechanical support. Recent reports on the native extracellular matrix platform and robust protocols for directed differentiation of human pluripotent stem cells provide key building blocks that could be combined towards that goal. Herein, we describe regeneration of functional human myocardial tissue constructs based on decellularized human cardiac ECM and human iPS-derived cardiac myocytes, and report four technical milestones that are paramount for bringing this technology closer to clinical relevance: the generation of biocompatible acellular whole organ scaffolds from discarded human donor hearts by perfusion decellularization, which elicit a more modulatory immunological response; the directed differentiation of adult derived, non-transgenic iPSC to generate cardiac myocytes at a clinical scale; the engraftment of human iPS derived cardiac myocytes on native ECM for the development of functionally contractile tissue; and the up-scaling to biomimetic organ culture to generate functional myocardial tissue in the context of a human heart.

Perfusion decellularization has been applied to hearts from several species[15, 33–35]. Through collaboration with the New England Organ Bank and thanks to the generous gift of organ donors and their families, we had access to hearts not used for transplantation. We followed a previously published detergent based perfusion decellularization protocol to generate scaffolds of reproducible characteristics[15, 36, 37]. In our studies, the increased warm ischemia time and potentially incomplete heparinization of DCD donors did not have any detectable detrimental effect on the decellularization process or the resulting scaffold when compared to hearts from DBD donors. This finding is of importance, given that approximately 1,600 DCD donor hearts are currently available per year in the US[3, 38], and this number is expected to increase[39–41]. While human donors represent a more heterogeneous pool compared to well-characterized porcine donor herds, current organ donation, allocation, and procurement infrastructures are well established, and donors undergo extensive screening to ensure freedom from pathogens. Furthermore, differences in anatomy and physiology between porcine and human hearts (e.g. shape, pulmonary venous anatomy) may prove to be relevant in regenerated myocardial grafts[42, 43]. From a regulatory perspective, perfusion decellularized human heart matrix could be a readily available and safe first step on a pathway towards clinical translation.

As has been reported in other human organs[44], decellularization of hearts with structural disease and atherosclerotic lesions yielded scaffolds with corresponding matrix defects. In line with prior work[15, 36, 45], we found preservation of a hierarchical network of macro- and microvascular channels after decellularization, providing the foundation for the formation of metabolically active myocardium. Our analysis revealed preserved vascular density and binned diameter distribution in decellularized myocardium compared to cadaveric controls

and data reported in human hearts and animal models[46, 47]. Using high resolution μCT imaging (6 μm), this finding extended to comparable lower-boundary density and distribution of small-diameter vessels (<80 μm) in decellularized and cadaveric hearts. Though there was no statistical difference found in vessel density across regions, decellularized hearts tended to demonstrate slightly lower densities, visibly noticeable in the μCT of mid- and endocardial regions. This presents a technical limitation, as the loss of endothelium and tissue-turgor make the recruitment of deeper vascular conduits more challenging. For culture of recellularized hearts, perfusion pressure must be increased towards the higher-end of physiological range in order to ensure media flow to reseeded regions. Active and passive mechanical properties of native myocardium are a result of mutually orthogonal fiber directions and play a key role in translating mechanical function from cells, to tissue, and to organ.[48]. In human hearts, perfusion decellularization did not affect the anisotropic behavior of myocardium upon passive mechanical testing, indicating the preservation of the native fiber framework within the myocardial matrix[49]. Artificial scaffolds designed to reproduce some of the anisotropic behavior of myocardial tissue have been repopulated with cardiac myocytes to create engineered myocardial tissue grafts with anisotropic properties[50, 51]. However, reproduction of the multidimensional complexity of native cardiac fiber architecture in a synthetic whole organ scaffold has not been accomplished to date. Based on our results we concluded that perfusion decellularization of whole human hearts captures a structural blueprint that could guide the formation of electrically and mechanically orthotropic myocardium.

In the present study, perfusion decellularization of human hearts resulted in acellular scaffolds consisting of major extracellular matrix components such as collagens, elastin, and glycosaminoglycans, which is in line with similar data published in other organ systems and species[15, 36, 37], and decellularized human heart sections[52]. Quantitative analyses of extracellular matrix components were similar in DCD and DBD hearts, with preservation of insoluble collagen and glycosaminoglycans, and reduction of soluble collagen and elastin. This is consistent with a loss of mainly immature collagen, while more mature, crosslinked, high-strength collagen is preserved[53]. Histological and immunohistochemical analysis showed absence of nuclei and cytoplasmic components such as myosin heavy chain. Further compositional analysis using mass spectrometry-based label-free proteomics revealed an 89.14% reduction of total protein content to 105 proteins and confirmed preservation of 36 matrisome proteins, including important structural proteins such as fibrillin-1, collagen IV, collagen VI, and laminin. The relevance of the observed low level of intracellular cardiac peptides within the cardiac scaffolds for recellularization and transplantation has yet to be determined. The potential clinical value of any organ matrix depends on complete removal of cell surface xeno- or allo-antigens, and substantial reduction of residual double stranded DNA. Perfusion decellularized human heart matrices contained less DNA than the currently accepted standard for biomesh implants, and could therefore be compatible with clinical transplantation[17]. We further confirmed absence of human leukocyte antigens by immunostaining of decellularized hearts, and the absence of antibody induction in an immunocompetent animal model *in vivo*. While we did not observe the generation of panel reactive antibodies, decellularized human heart matrixes promoted a CD163 heavy macrophage response, consistent with reconstructive remodeling described in non-

crosslinked, decellularized matrix implants[23, 54–56]. Notably, decellularized porcine myocardium showed a similar immunogenic profile as decellularized human myocardium by histology, although we did not examine the humoral response to porcine matrix. These early results hold promise from a device perspective, since in vivo remodeling and graft homeostasis will depend on the absence of chronic inflammation and the promotion of a reconstructive response[57].

Since induced pluripotent stem cells were first described, the generation of human iPS-derived cardiac myocytes holds immediate promise for cardiac applications[58, 59]. In cardiac regeneration, techniques have been developed for the delivery of human iPS-derived cardiac myocytes to improve cardiac function post-infarct[7, 60], provide cardioprotection[61], and enhance homing and survival in infarcted myocardium[62]. These approaches build on the extensive body of literature on ES derived cardiac myocytes, which have been recently reported to mediate myogenesis in a primate model of cardiac repair[32]. In parallel, the field of myocardial tissue engineering has provided a solid foundation for protocols to repopulate various scaffold materials with human iPS-derived cardiac myocytes and create functional tissue[7, 34, 63–66]. Our intent was to combine the techniques of directed differentiation and the principles of myocardial engineering to generate human myocardial grafts of clinical relevance, for applications in high-throughput screening and as a foundational basis for creating human myocardial grafts of clinically relevant scale.

With potential translation in mind, we chose to derive cardiac myocytes from a non-genetically altered pluripotent cell source that could be generated from patient-derived somatic cells via repeated administration of synthetic messenger RNAs[67, 68].. This method is characterized by lack of vector integration, high efficiency, and low rate of chromosomal abnormalities, and has been validated by several human reprogramming laboratories[69]. In order to generate cardiac myocytes at a clinically relevant scale, we adapted a directed differentiation protocol based on temporal modulation of canonical Wnt/β-catenin signaling to BJ RiPS cultured in monolayer[25]. This method yielded $5x10^8$ cardiac myocytes with reasonable use of resources and workload in the setting of an academic laboratory. In vitro differentiation of pluripotent stem cells recapitulates the sequential stages of embryonic cardiac development[70]. Therefore, with Wnt/β-catenin signaling[25], we identified definitive stages for the development of precardiac mesoderm (day 3), cardiac mesoderm (day 5), heart field specific progenitors (day 7), and iPS-derived cardiac myocytes (days 14, 30, 60, 120, and 180). While embryoid body methods have been applied to this cell line previously[71], we show that this protocol is highly reproducible for the cardiac differentiation of BJ RiPS, and demonstrates a facile method to generate a clinical number of cardiac myocytes with a high efficiency.

Using three-dimensional models of increasing complexity we were then able to document the formation of mechanically and electrically active myocardial tissue. In slice experiments, we first confirmed biocompatibility, cell-mediated matrix deformation, and force generation. The formation of contractile tissue on myocardial slices is evidence of reestablishment of cell-cell adhesions, as well as cell matrix coupling, which are essential features of the myocardial microenvironment[72]. Despite being a stationary model, the observed development of strain and force generation in cardiac slices further confirms that native

ECM provides a physiologic microenvironment known to be beneficial to pluripotent cell-derived cardiac myocytes and myofibers[13, 73]. In a second set of experiments, we scaled native ECM recellularization to myofibers of 15 mm in length and 2.5 mm in diameter. An improvement to stationary slices, but still non-perfused, the resulting tissue showed improved cell engraftment and orientation, increased strain and force generation, electrical conductivity, and improved fiber microarchitecture. This is in line with the observation that physiologic substrate stiffness improves contractility of neonatal and iPSC derived cardiac myocytes[74, 75]. The observed improvement in dynamic electrical and mechanical tissue function in fibers may further be related to improved rigidity matching and resulting cardiac myocytes-tissue synchronization within the native cardiac ECM[76].

Generation of tissue constructs of clinical value, either as whole heart grafts or myocardial implants ultimately requires regeneration of human myocardium on a whole organ scale [32, 63, 77, 78]. We therefore attempted tissue assembly in whole human heart matrices similar to prior reports in rat and mouse hearts[15, 79]. Depending on its size, nearly one billion cardiac myocytes are lost due to a myocardial infarction (MI)[80], while several billion cardiac myocytes would be required to completely repopulate an acellular human heart. To examine the clinical feasibility of myocardial regeneration, we attempted to deliver ~500 million cardiac myocytes to a highly vascularized ~5 cm^3 volume of the left ventricle, between the left anterior descending and left circumflex coronary arteries. Efficient cell delivery with minimal matrix damage could be achieved via five injections to multiple depths within the ventricular wall over a square epicardial region (Fig. 6E).

To enable tissue development, we designed and built a biomimetic bioreactor system to accommodate whole heart scaffolds, largely based on reported isolated working heart models, and the well documented role of mechanical stimulation in the formation of myocardial tissue constructs[81–84]. Media perfusion via the native coronary vascular channels provided sufficient nutrient and oxygen supply to enable the formation of myocardial tissue within the context of the whole heart scaffold. After a culture period of 14 days, repopulated myocardial segments were metabolically active, provided contractile function, and responded to electrical stimulation. Myocardial tissue was immature, showing a range of rounded to elongated sarcomeric phenotypes, which corresponds to reported morphologic features of developing myocardium[85, 86] and the in vivo fate of pluripotent cell derived cardiac myocytes[87]. This endpoint was chosen based on the need to analyze cell viability and tissue formation, however, full maturation will likely require longer culture times and improved biomimetic regimens.

While we believe that the present data set proves the translational value of the human acellular matrix platform and the ability to generate myocardial tissue of clinically relevant origin and platform, the present experiments did not aim to achieve full recellularization of the myocardium of an entire human heart. Several challenges lie ahead in bringing this technology to clinical scale and applications. Full recellularization of the myocardial matrix and valve structures are necessary for generating sustainable ventricular pump function. Achieving this necessitates improved recellularization techniques to enhance cell coverage without damaging the matrix (*e.g.* uni-directional or bi-directional vascular techniques). Additionally, biomimetic culture conditions (*i.e.* static or dynamic stretch, electrical

stimulation, media components) must be optimized to elicit the maturity of reseeded cardiac myocytes and drive tissue development. Considerations should potentially be made to donor matrix age and composition, for the promotion of improved cell-matrix integration. A larger-scale immunological study is needed for a more complete understanding host-response to cardiac matrices over time, as well as to understand the modulatory or reconstructive effects on the matrix. Importantly, techniques to achieve and test for complete re-endothelialization are critical in clinical application for the maintenance of blood-flow throughout the organ (*i.e.* vascular recruitment) and to prevent matrix-induced blood coagulation. The present study provides a foundational toolset to generate grafts of human scale for therapeutic applications, and multiple model platforms to generate patient derived human myocardium of different scales for analytical purposes. Undoubtedly, many hurdles towards the regeneration of whole heart grafts remain, including the need for complete re-endothelialization, repopulation of the valvular apparatus, and re-establishment of a functional conduction system.

Supplementary Material

Refer to Web version on PubMed Central for supplementary material.

Acknowledgments

We thank the New England Organ Bank and all of the explant surgeons for their continued support and coordination involved in organ procurement. We further thank the Program in Membrane Biology Microscopy Core at MGH, as well as Ann Tisdale at the MEEI, for technical support with scanning electron microscopy (supported by NIH grants DK43351 and DK57521). We thank Jeremy Song, MD for his contributions to decellularization process development. Additionally, we thank Wenpo Chuang, MD and Roger Ng, MD for their contributions to cardiac angiography. We thank TuKiet Lam, PhD and his team at the MS & Proteomics Resource at Yale School of Medicine for support with proteomics analysis, as well as James Titus and Chris Owen at MGH for support and use of fluoroscopy suites. We further thank John Favreau, PhD for program support involved with HDM functional analysis. We thank Patricia Della Pelle, Gertraude Warren, Jed Barger, and Susan Saidman, PhD for their help with immunogenic profiling and HLA testing. For vascular analysis, we thank Brian Ghoshhajra, MD in the Department of Radiology at MGH. Further, we thank Daniel Brooks, Mathew Scott, and Adriana Martinez-Betancourt in the Center for Advanced Orthopedic Studies at Beth Israel Deaconess Medical Center for their assistance with microcomputed tomography of microvasculature. In addition, we would like to thank Megan Scanlan for her assistance with transmission electron microscopy on cardiac fibers. Lastly, we want to thank Kengyeh Chu, PhD and Joseph Gardecki, PhD of the Wellman Center for Photomedicine at MGH, for their assistance with micro-optical coherence tomography on cardiac fibers and microvasculature.

SOURCES OF FUNDING

The present study was supported by the US National Institutes of Health (NIH) Director's New Innovator DP2 OD008749-01, and by the National Heart Lung and Blood Institute R21 HL108663-2 and R01 HL115282.

Nonstandard Abbreviations and Acronyms

ECM	extracellular matrix
DCD	donation after cardiac death
DBD	donation after brain death
iPSC	induced pluripotent stem cell
BJ-RiPS	BJ fibroblast RNA-induced pluripotent stem

μOCT	micro-optical coherence tomography
APD80	action potential duration at 80%
MFI	mean fluorescence intensity
HDM	high density mapping
TTRX	time to X% relaxation
μCT	micro-computed tomography
SDS	sodium dodecyl sulfate (cells)
HLA	human leukocyte antigen

References

1. Go AS, Mozaffarian D, Roger VL, Benjamin EJ, Berry JD, Blaha MJ, Dai S, Ford ES, Fox CS, Franco S, Fullerton HJ, Gillespie C, Hailpern SM, Heit JA, Howard VJ, Huffman MD, Judd SE, Kissela BM, Kittner SJ, Lackland DT, Lichtman JH, Lisabeth LD, Mackey RH, Magid DJ, Marcus GM, Marelli A, Matchar DB, McGuire DK, Mohler ER 3rd, Moy CS, Mussolino ME, Neumar RW, Nichol G, Pandey DK, Paynter NP, Reeves MJ, Sorlie PD, Stein J, Towfighi A, Turan TN, Virani SS, Wong ND, Woo D, Turner MB. Heart disease and stroke statistics--2014 update: A report from the american heart association. Circulation. 2014; 129:e28–e292. [PubMed: 24352519]
2. Braunwald E. Heart failure. JACC. Heart failure. 2013; 1:1–20. [PubMed: 24621794]
3. Organ procurement and transplantation network (optn) - national data reports; u.S. Department of health and human services, health resources services administration (hrsa). 2014
4. Tonsho M, Michel S, Ahmed Z, Alessandrini A, Madsen JC. Heart transplantation: Challenges facing the field. Cold Spring Harbor perspectives in medicine. 2014; 4
5. Hill JA, Olson EN. Cardiac plasticity. N Engl J Med. 2008; 358:1370–1380. [PubMed: 18367740]
6. Chong JJ, Yang X, Don CW, Minami E, Liu YW, Weyers JJ, Mahoney WM, Van Biber B, Palpant NJ, Gantz JA, Fugate JA, Muskheli V, Gough GM, Vogel KW, Astley CA, Hotchkiss CE, Baldessari A, Pabon L, Reinecke H, Gill EA, Nelson V, Kiem HP, Laflamme MA, Murry CE. Human embryonic-stem-cell-derived cardiac myocytes regenerate non-human primate hearts. Nature. 2014
7. Kawamura M, Miyagawa S, Miki K, Saito A, Fukushima S, Higuchi T, Kawamura T, Kuratani T, Daimon T, Shimizu T, Okano T, Sawa Y. Feasibility, safety, and therapeutic efficacy of human induced pluripotent stem cell-derived cardiac myocyte sheets in a porcine ischemic cardiomyopathy model. Circulation. 2012; 126:S29–37. [PubMed: 22965990]
8. Seif-Naraghi SB, Singelyn JM, Salvatore MA, Osborn KG, Wang JJ, Sampat U, Kwan OL, Strachan GM, Wong J, Schup-Magoffin PJ, Braden RL, Bartels K, DeQuach JA, Preul M, Kinsey AM, DeMaria AN, Dib N, Christman KL. Safety and efficacy of an injectable extracellular matrix hydrogel for treating myocardial infarction. Science translational medicine. 2013; 5:173ra125.
9. Leor J, Tuvia S, Guetta V, Manczur F, Castel D, Willenz U, Petnehazy O, Landa N, Feinberg MS, Konen E, Goitein O, Tsur-Gang O, Shaul M, Klapper L, Cohen S. Intracoronary injection of in situ forming alginate hydrogel reverses left ventricular remodeling after myocardial infarction in swine. J Am Coll Cardiol. 2009; 54:1014–1023. [PubMed: 19729119]
10. Coulombe KL, Bajpai VK, Andreadis ST, Murry CE. Heart regeneration with engineered myocardial tissue. Annu Rev Biomed Eng. 2014
11. Zimmermann WH, Melnychenko I, Eschenhagen T. Engineered heart tissue for regeneration of diseased hearts. Biomaterials. 2004; 25:1639–1647. [PubMed: 14697865]
12. Radisic M, Deen W, Langer R, Vunjak-Novakovic G. Mathematical model of oxygen distribution in engineered cardiac tissue with parallel channel array perfused with culture medium containing

oxygen carriers. American journal of physiology. Heart and circulatory physiology. 2005; 288:H1278–1289. [PubMed: 15539422]

13. Engler AJ, Carag-Krieger C, Johnson CP, Raab M, Tang HY, Speicher DW, Sanger JW, Sanger JM, Discher DE. Embryonic cardiac myocytes beat best on a matrix with heart-like elasticity: Scar-like rigidity inhibits beating. Journal of cell science. 2008; 121:3794–3802. [PubMed: 18957515]
14. Buckberg G, Hoffman JI, Mahajan A, Saleh S, Coghlan C. Cardiac mechanics revisited: The relationship of cardiac architecture to ventricular function. Circulation. 2008; 118:2571–2587. [PubMed: 19064692]
15. Ott HC, Matthiesen TS, Goh SK, Black LD, Kren SM, Netoff TI, Taylor DA. Perfusion-decellularized matrix: Using nature's platform to engineer a bioartificial heart. Nat Med. 2008; 14:213–221. [PubMed: 18193059]
16. Guyette JP, Gilpin SE, Charest JM, Tapias LF, Ren X, Ott HC. Perfusion decellularization of whole organs. Nature protocols. 2014; 9:1451–1468. [PubMed: 24874812]
17. Crapo PM, Gilbert TW, Badylak SF. An overview of tissue and whole organ decellularization processes. Biomaterials. 2011; 32:3233–3243. [PubMed: 21296410]
18. Rusconi F, Valton E, Nguyen R, Dufourc E. Quantification of sodium dodecyl sulfate in microliter-volume biochemical samples by visible light spectroscopy. Analytical biochemistry. 2001; 295:31–37. [PubMed: 11476542]
19. Magrane M. Consortium U. Uniprot knowledgebase: A hub of integrated protein data. Database : the journal of biological databases and curation. 2011; 2011:bar009. [PubMed: 21447597]
20. Ashburner M, Ball CA, Blake JA, Botstein D, Butler H, Cherry JM, Davis AP, Dolinski K, Dwight SS, Eppig JT, Harris MA, Hill DP, Issel-Tarver L, Kasarskis A, Lewis S, Matese JC, Richardson JE, Ringwald M, Rubin GM, Sherlock G. Gene ontology: Tool for the unification of biology. The gene ontology consortium. Nature genetics. 2000; 25:25–29. [PubMed: 10802651]
21. Carpenter AE, Jones TR, Lamprecht MR, Clarke C, Kang IH, Friman O, Guertin DA, Chang JH, Lindquist RA, Moffat J, Golland P, Sabatini DM. Cellprofiler: Image analysis software for identifying and quantifying cell phenotypes. Genome biology. 2006; 7:R100. [PubMed: 17076895]
22. Jones TR, Carpenter AE, Lamprecht MR, Moffat J, Silver SJ, Grenier JK, Castoreno AB, Eggert US, Root DE, Golland P, Sabatini DM. Scoring diverse cellular morphologies in image-based screens with iterative feedback and machine learning. Proc Natl Acad Sci U S A. 2009; 106:1826–1831. [PubMed: 19188593]
23. Badylak SF, Valentin JE, Ravindra AK, McCabe GP, Stewart-Akers AM. Macrophage phenotype as a determinant of biologic scaffold remodeling. Tissue Eng Part A. 2008; 14:1835–1842. [PubMed: 18950271]
24. Warren L, Manos PD, Ahfeldt T, Loh YH, Li H, Lau F, Ebina W, Mandal PK, Smith ZD, Meissner A, Daley GQ, Brack AS, Collins JJ, Cowan C, Schlaeger TM, Rossi DJ. Highly efficient reprogramming to pluripotency and directed differentiation of human cells with synthetic modified mrna. Cell stem cell. 2010; 7:618–630. [PubMed: 20888316]
25. Lian X, Hsiao C, Wilson G, Zhu K, Hazeltine LB, Azarin SM, Raval KK, Zhang J, Kamp TJ, Palecek SP. Robust cardiac myocyte differentiation from human pluripotent stem cells via temporal modulation of canonical wnt signaling. Proc Natl Acad Sci U S A. 2012; 109:E1848–1857. [PubMed: 22645348]
26. Kelly DJ, Azeloglu EU, Kochupura PV, Sharma GS, Gaudette GR. Accuracy and reproducibility of a subpixel extended phase correlation method to determine micron level displacements in the heart. Med Eng Phys. 2007; 29:154–162. [PubMed: 16531092]
27. Kochupura PV, Azeloglu EU, Kelly DJ, Doronin SV, Badylak SF, Krukenkamp IB, Cohen IS, Gaudette GR. Tissue-engineered myocardial patch derived from extracellular matrix provides regional mechanical function. Circulation. 2005; 112:I144–149. [PubMed: 16159807]
28. Liu L, Gardecki JA, Nadkarni SK, Toussaint JD, Yagi Y, Bouma BE, Tearney GJ. Imaging the subcellular structure of human coronary atherosclerosis using micro-optical coherence tomography. Nat Med. 2011; 17:1010–1014. [PubMed: 21743452]

29. Liu J, Sun N, Bruce MA, Wu JC, Butte MJ. Atomic force mechanobiology of pluripotent stem cell-derived cardiac myocytes. PLoS ONE. 2012; 7:e37559. [PubMed: 22624048]
30. Rodriguez, MLMC.; Sniadecki, NJ. Assessment of induced pluripotent stem cell-derived cardiac myocyte contractility using micropost arrays. ASME 2013 Summer Bioengineering Conference; SBC2013–14640; 2013. p. V01AT15A005
31. Xi J, Khalil M, Shishechian N, Hannes T, Pfannkuche K, Liang H, Fatima A, Haustein M, Suhr F, Bloch W, Reppel M, Saric T, Wernig M, Janisch R, Brockmeier K, Hescheler J, Pillekamp F. Comparison of contractile behavior of native murine ventricular tissue and cardiac myocytes derived from embryonic or induced pluripotent stem cells. Faseb J. 2010; 24:2739–2751. [PubMed: 20371616]
32. Chong JJ, Yang X, Don CW, Minami E, Liu YW, Weyers JJ, Mahoney WM, Van Biber B, Cook SM, Palpant NJ, Gantz JA, Fugate JA, Muskheli V, Gough GM, Vogel KW, Astley CA, Hotchkiss CE, Baldessari A, Pabon L, Reinecke H, Gill EA, Nelson V, Kiem HP, Laflamme MA, Murry CE. Human embryonic-stem-cell-derived cardiac myocytes regenerate non-human primate hearts. Nature. 2014; 510:273–277. [PubMed: 24776797]
33. Wainwright JM, Czajka CA, Patel UB, Freytes DO, Tobita K, Gilbert TW, Badylak SF. Preparation of cardiac extracellular matrix from an intact porcine heart. Tissue engineering. Part C, Methods. 2010; 16:525–532. [PubMed: 19702513]
34. Lu TY, Lin B, Kim J, Sullivan M, Tobita K, Salama G, Yang L. Repopulation of decellularized mouse heart with human induced pluripotent stem cell-derived cardiovascular progenitor cells. Nat Commun. 2013; 4:2307. [PubMed: 23942048]
35. Sanchez PL, Fernandez-Santos ME, Costanza S, Climent AM, Moscoso I, Gonzalez-Nicolas MA, Sanz-Ruiz R, Rodriguez H, Kren SM, Garrido G, Escalante JL, Bermejo J, Elizaga J, Menarguez J, Yotti R, Perez del Villar C, Espinosa MA, Guillem MS, Willerson JT, Bernad A, Matesanz R, Taylor DA, Fernandez-Aviles F. Acellular human heart matrix: A critical step toward whole heart grafts. Biomaterials. 2015; 61:279–289. [PubMed: 26005766]
36. Song JJ, Guyette JP, Gilpin SE, Gonzalez G, Vacanti JP, Ott HC. Regeneration and experimental orthotopic transplantation of a bioengineered kidney. Nat Med. 2013; 19:646–651. [PubMed: 23584091]
37. Gilpin SE, Guyette JP, Gonzalez G, Ren X, Asara JM, Mathisen DJ, Vacanti JP, Ott HC. Perfusion decellularization of human and porcine lungs: Bringing the matrix to clinical scale. J Heart Lung Transplant. 2014; 33:298–308. [PubMed: 24365767]
38. Osaki S, Anderson JE, Johnson MR, Edwards NM, Kohmoto T. The potential of cardiac allografts from donors after cardiac death at the university of wisconsin organ procurement organization. Eur J Cardiothorac Surg. 2010; 37:74–79. [PubMed: 19695894]
39. Zych B, Popov AF, Amrani M, Bahrami T, Redmond KC, Krueger H, Carby M, Simon AR. Lungs from donation after circulatory death donors: An alternative source to brain-dead donors? Midterm results at a single institution. Eur J Cardiothorac Surg. 2012; 42:542–549. [PubMed: 22371518]
40. Alvarez J, del Barrio R, Arias J, Vazquez S, Sanchez A, Iglesias J, Barra C, Ibarguren C. Non-heart-beating donors: Estimated actual potential. Transplantation proceedings. 2001; 33:1101–1103. [PubMed: 11267209]
41. Garcia Saez D, Elbetanony A, Lezberg P, Hassanein A, Bowles CT, Popov AF, Zych B, Sabashnikov A, Mohite P, Simon AR. Ex vivo heart perfusion after cardiocirculatory death; a porcine model. J Surg Res. 2014
42. Crick SJ, Sheppard MN, Ho SY, Gebstein L, Anderson RH. Anatomy of the pig heart: Comparisons with normal human cardiac structure. J Anat. 1998; 193(Pt 1):105–119. [PubMed: 9758141]
43. Lelovas PP, Kostomitsopoulos NG, Xanthos TT. A comparative anatomic and physiologic overview of the porcine heart. Journal of the American Association for Laboratory Animal Science : JAALAS. 2014; 53:432–438. [PubMed: 25255064]
44. Sokocevic D, Bonenfant NR, Wagner DE, Borg ZD, Lathrop MJ, Lam YW, Deng B, Desarno MJ, Ashikaga T, Loi R, Hoffman AM, Weiss DJ. The effect of age and emphysematous and fibrotic injury on the re-cellularization of de-cellularized lungs. Biomaterials. 2013; 34:3256–3269. [PubMed: 23384794]

45. Ott HC, Clippinger B, Conrad C, Schuetz C, Pomerantseva I, Ikonomou L, Kotton D, Vacanti JP. Regeneration and orthotopic transplantation of a bioartificial lung. Nat Med. 2010; 16:927–933. [PubMed: 20628374]

46. Rodriguez-Porcel M, Lerman A, Ritman EL, Wilson SH, Best PJ, Lerman LO. Altered myocardial microvascular 3d architecture in experimental hypercholesterolemia. Circulation. 2000; 102:2028–2030. [PubMed: 11044415]

47. Sangaralingham SJ, Ritman EL, McKie PM, Ichiki T, Lerman A, Scott CG, Martin FL, Harders GE, Bellavia D, Burnett JC Jr. Cardiac micro-computed tomography imaging of the aging coronary vasculature. Circulation. Cardiovascular imaging. 2012; 5:518–524. [PubMed: 22679058]

48. Cansiz FB, Dal H, Kaliske M. An orthotropic viscoelastic material model for passive myocardium: Theory and algorithmic treatment. Computer methods in biomechanics and biomedical engineering. 2015; 18:1160–1172. [PubMed: 24533658]

49. Holzapfel GA, Ogden RW. Constitutive modelling of passive myocardium: A structurally based framework for material characterization. Philosophical transactions. Series A, Mathematical, physical, and engineering sciences. 2009; 367:3445–3475.

50. Engelmayr GC Jr, Cheng M, Bettinger CJ, Borenstein JT, Langer R, Freed LE. Accordion-like honeycombs for tissue engineering of cardiac anisotropy. Nat Mater. 2008; 7:1003–1010. [PubMed: 18978786]

51. Costa KD, Lee EJ, Holmes JW. Creating alignment and anisotropy in engineered heart tissue: Role of boundary conditions in a model three-dimensional culture system. Tissue Eng. 2003; 9:567–577. [PubMed: 13678436]

52. Oberwallner B, Brodarac A, Choi YH, Saric T, Anic P, Morawietz L, Stamm C. Preparation of cardiac extracellular matrix scaffolds by decellularization of human myocardium. J Biomed Mater Res A. 2014; 102:3263–3272. [PubMed: 24142588]

53. Friess W. Collagen--biomaterial for drug delivery. European journal of pharmaceutics and biopharmaceutics : official journal of Arbeitsgemeinschaft fur Pharmazeutische Verfahrenstechnik e. V. 1998; 45:113–136. [PubMed: 9704909]

54. Badylak SF, Gilbert TW. Immune response to biologic scaffold materials. Seminars in immunology. 2008; 20:109–116. [PubMed: 18083531]

55. Brown BN, Londono R, Tottey S, Zhang L, Kukla KA, Wolf MT, Daly KA, Reing JE, Badylak SF. Macrophage phenotype as a predictor of constructive remodeling following the implantation of biologically derived surgical mesh materials. Acta biomaterialia. 2012; 8:978–987. [PubMed: 22166681]

56. Brown BN, Ratner BD, Goodman SB, Amar S, Badylak SF. Macrophage polarization: An opportunity for improved outcomes in biomaterials and regenerative medicine. Biomaterials. 2012; 33:3792–3802. [PubMed: 22386919]

57. Ariganello MB, Simionescu DT, Labow RS, Lee JM. Macrophage differentiation and polarization on a decellularized pericardial biomaterial. Biomaterials. 2011; 32:439–449. [PubMed: 20933269]

58. Takahashi K, Tanabe K, Ohnuki M, Narita M, Ichisaka T, Tomoda K, Yamanaka S. Induction of pluripotent stem cells from adult human fibroblasts by defined factors. Cell. 2007; 131:861–872. [PubMed: 18035408]

59. Zhang J, Wilson GF, Soerens AG, Koonce CH, Yu J, Palecek SP, Thomson JA, Kamp TJ. Functional cardiac myocytes derived from human induced pluripotent stem cells. Circ Res. 2009; 104:e30–41. [PubMed: 19213953]

60. Citro L, Naidu S, Hassan F, Kuppusamy ML, Kuppusamy P, Angelos MG, Khan M. Comparison of human induced pluripotent stem-cell derived cardiac myocytes with human mesenchymal stem cells following acute myocardial infarction. PLoS ONE. 2014; 9:e116281. [PubMed: 25551230]

61. Carpenter L, Carr C, Yang CT, Stuckey DJ, Clarke K, Watt SM. Efficient differentiation of human induced pluripotent stem cells generates cardiac cells that provide protection following myocardial infarction in the rat. Stem cells and development. 2012; 21:977–986. [PubMed: 22182484]

62. Malecki M, Putzer E, Sabo C, Foorohar A, Quach C, Stampe C, Beauchaine M, Malecki R, Tombokan X, Anderson M. Directed cardiomyogenesis of autologous human induced pluripotent

stem cells recruited to infarcted myocardium with bioengineered antibodies. Molecular and cellular therapies. 2014; 2

63. Kawamura M, Miyagawa S, Fukushima S, Saito A, Miki K, Ito E, Sougawa N, Kawamura T, Daimon T, Shimizu T, Okano T, Toda K, Sawa Y. Enhanced survival of transplanted human induced pluripotent stem cell-derived cardiac myocytes by the combination of cell sheets with the pedicled omental flap technique in a porcine heart. Circulation. 2013; 128:S87–94. [PubMed: 24030425]
64. Masumoto H, Ikuno T, Takeda M, Fukushima H, Marui A, Katayama S, Shimizu T, Ikeda T, Okano T, Sakata R, Yamashita JK. Human ips cell-engineered cardiac tissue sheets with cardiac myocytes and vascular cells for cardiac regeneration. Scientific reports. 2014; 4:6716. [PubMed: 25336194]
65. Masumoto H, Matsuo T, Yamamizu K, Uosaki H, Narazaki G, Katayama S, Marui A, Shimizu T, Ikeda T, Okano T, Sakata R, Yamashita JK. Pluripotent stem cell-engineered cell sheets reassembled with defined cardiovascular populations ameliorate reduction in infarct heart function through cardiac myocyte-mediated neovascularization. Stem Cells. 2012; 30:1196–1205. [PubMed: 22438013]
66. Fujita J, Itabashi Y, Seki T, Tohyama S, Tamura Y, Sano M, Fukuda K. Myocardial cell sheet therapy and cardiac function. Am J Physiol Heart Circ Physiol. 2012; 303:H1169–1182. [PubMed: 23001836]
67. Warren L, Manos PD, Ahfeldt T, Loh Y-H, Li H, Lau F, Ebina W, Mandal PK, Smith ZD, Meissner A, Daley GQ, Brack AS, Collins JJ, Cowan C, Schlaeger TM, Rossi DJ. Highly efficient reprogramming to pluripotency and directed differentiation of human cells with synthetic modified mrna. Cell stem cell. 2010; 7:618–630. [PubMed: 20888316]
68. Soares FA, Sheldon M, Rao M, Mummery C, Vallier L. International coordination of large-scale human induced pluripotent stem cell initiatives: Wellcome trust and isscr workshops white paper. Stem cell reports. 2014; 3:931–939. [PubMed: 25496616]
69. Schlaeger TM, Daheron L, Brickler TR, Entwisle S, Chan K, Cianci A, DeVine A, Ettenger A, Fitzgerald K, Godfrey M, Gupta D, McPherson J, Malwadkar P, Gupta M, Bell B, Doi A, Jung N, Li X, Lynes MS, Brookes E, Cherry AB, Demirbas D, Tsankov AM, Zon LI, Rubin LL, Feinberg AP, Meissner A, Cowan CA, Daley GQ. A comparison of non-integrating reprogramming methods. Nat Biotechnol. 2015; 33:58–63. [PubMed: 25437882]
70. Mummery CL, Zhang J, Ng ES, Elliott DA, Elefanty AG, Kamp TJ. Differentiation of human embryonic stem cells and induced pluripotent stem cells to cardiac myocytes: A methods overview. Circ Res. 2012; 111:344–358. [PubMed: 22821908]
71. Mehta A, Verma V, Nandihalli M, Ramachandra CJ, Sequiera GL, Sudibyo Y, Chung Y, Sun W, Shim W. A systemic evaluation of cardiac differentiation from mrna reprogrammed human induced pluripotent stem cells. PLoS ONE. 2014; 9:e103485. [PubMed: 25068310]
72. McCain ML, Lee H, Aratyn-Schaus Y, Kleber AG, Parker KK. Cooperative coupling of cell-matrix and cell-cell adhesions in cardiac muscle. Proc Natl Acad Sci U S A. 2012; 109:9881–9886. [PubMed: 22675119]
73. Engler AJ, Griffin MA, Sen S, Bonnemann CG, Sweeney HL, Discher DE. Myotubes differentiate optimally on substrates with tissue-like stiffness: Pathological implications for soft or stiff microenvironments. J Cell Biol. 2004; 166:877–887. [PubMed: 15364962]
74. Rodriguez AG, Han SJ, Regnier M, Sniadecki NJ. Substrate stiffness increases twitch power of neonatal cardiac myocytes in correlation with changes in myofibril structure and intracellular calcium. Biophys J. 2011; 101:2455–2464. [PubMed: 22098744]
75. Marsano A, Maidhof R, Wan LQ, Wang Y, Gao J, Tandon N, Vunjak-Novakovic G. Scaffold stiffness affects the contractile function of three-dimensional engineered cardiac constructs. Biotechnol Prog. 2010; 26:1382–1390. [PubMed: 20945492]
76. Horning M, Kidoaki S, Kawano T, Yoshikawa K. Rigidity matching between cells and the extracellular matrix leads to the stabilization of cardiac conduction. Biophys J. 2012; 102:379–387. [PubMed: 22325259]
77. Shiba Y, Fernandes S, Zhu WZ, Filice D, Muskheli V, Kim J, Palpant NJ, Gantz J, Moyes KW, Reinecke H, Van Biber B, Dardas T, Mignone JL, Izawa A, Hanna R, Viswanathan M, Gold JD, Kotlikoff MI, Sarvazyan N, Kay MW, Murry CE, Laflamme MA. Human es-cell-derived cardiac

myocytes electrically couple and suppress arrhythmias in injured hearts. Nature. 2012; 489:322–325. [PubMed: 22864415]

78. Zhang F, Song G, Li X, Gu W, Shen Y, Chen M, Yang B, Qian L, Cao K. Transplantation of ipsc ameliorates neural remodeling and reduces ventricular arrhythmias in a post-infarcted swine model. J Cell Biochem. 2014; 115:531–539. [PubMed: 24122925]
79. Lu T-Y, Lin B, Kim J, Sullivan M, Tobita K, Salama G, Yang L. Repopulation of decellularized mouse heart with human induced pluripotent stem cell-derived cardiovascular progenitor cells. Nat Commun. 2013; 4
80. Laflamme MA, Murry CE. Regenerating the heart. Nat Biotechnol. 2005; 23:845–856. [PubMed: 16003373]
81. Hill AJ, Laske TG, Coles JA Jr, Sigg DC, Skadsberg ND, Vincent SA, Soule CL, Gallagher WJ, Iaizzo PA. In vitro studies of human hearts. Ann Thorac Surg. 2005; 79:168–177. [PubMed: 15620938]
82. Hulsmann J, Aubin H, Kranz A, Godehardt E, Munakata H, Kamiya H, Barth M, Lichtenberg A, Akhyari P. A novel customizable modular bioreactor system for whole-heart cultivation under controlled 3d biomechanical stimulation. Journal of artificial organs : the official journal of the Japanese Society for Artificial Organs. 2013; 16:294–304. [PubMed: 23588844]
83. Wang B, Wang G, To F, Butler JR, Claude A, McLaughlin RM, Williams LN, de Jongh Curry AL, Liao J. Myocardial scaffold-based cardiac tissue engineering: Application of coordinated mechanical and electrical stimulations. Langmuir : the ACS journal of surfaces and colloids. 2013; 29:11109–11117. [PubMed: 23923967]
84. Vunjak-Novakovic G, Tandon N, Godier A, Maidhof R, Marsano A, Martens TP, Radisic M. Challenges in cardiac tissue engineering. Tissue Engineering Part B: Reviews. 2010; 16:169–187. [PubMed: 19698068]
85. Du A, Sanger JM, Sanger JW. Cardiac myofibrillogenesis inside intact embryonic hearts. Dev Biol. 2008; 318:236–246. [PubMed: 18455713]
86. Yang X, Pabon L, Murry CE. Engineering adolescence: Maturation of human pluripotent stem cell-derived cardiac myocytes. Circ Res. 2014; 114:511–523. [PubMed: 24481842]
87. Lundy SD, Zhu WZ, Regnier M, Laflamme MA. Structural and functional maturation of cardiac myocytes derived from human pluripotent stem cells. Stem cells and development. 2013; 22:1991–2002. [PubMed: 23461462]

NOVELTY AND SIGNIFICANCE

What Is Known?

- Currently, heart transplantation remains the only curative option for replacing necrotic cardiac tissue and sustaining longer-term survival in patients with heart failure.
- The creation of bioengineered myocardium, either in the form of a cardiac tissue graft or a bioartificial heart, theoretically holds the promise to improve contractile function to the injured heart.

What New Information Does This Article Contribute?

- Human hearts were decellularized using aseptic pressure-controlled perfusion to create acellular cardiac scaffolds with preserved extracellular matrix components, architecture, material properties, and microvasculature.
- Characterization of the acellular human scaffolds with thorough proteomics, microvasculature, and immunogenicity analyses.
- Human cardiac myocytes were derived from a non-transgenic induced pluripotent stem cell line, to generate cardiac myocytes at a clinically relevant scale, and create force-generating human myocardial-like tissue slices, fibers, and ventricular segments on whole-heart scaffolds.

In a first step towards the creation of bioartificial myocardium, we sought to engineer myocardial tissue that combines acellular human cardiac matrix and clinically relevant human iPS-derived cardiac myocytes. We used a new pressure-controlled perfusion system to aseptically decellularize human hearts. The resulting acellular human cardiac scaffolds were void of cellular material, while maintaining matrisomal content and extracellular matrix structure. Immunogenicity studies confirmed the removal of human leukocyte antigens, while also eliciting a reconstructive remodeling response when implanted in vivo. Casting analysis determined that acellular scaffolds contained a preserved microvasculature, with a vessel distribution similar to cadaveric hearts. Using a directed cardiac differentiation protocol on a non-transgenic induced pluripotent stem (iPS) cell line, we generated a clinically relevant number of human cardiac myocytes. We then reseeded acellular human cardiac matrix with human iPS-derived cardiac myocytes to create force-generating myocardial-like tissues of increasing three-dimensional complexity. Recellularized cardiac slices and fibers could be maintained for 120 days in culture, showing increased sarcomeric structure and electromechanical function. We then upscaled these techniques to partially recellularize intact hearts, to show that functional myocardial tissue could be built on a whole-heart platform.

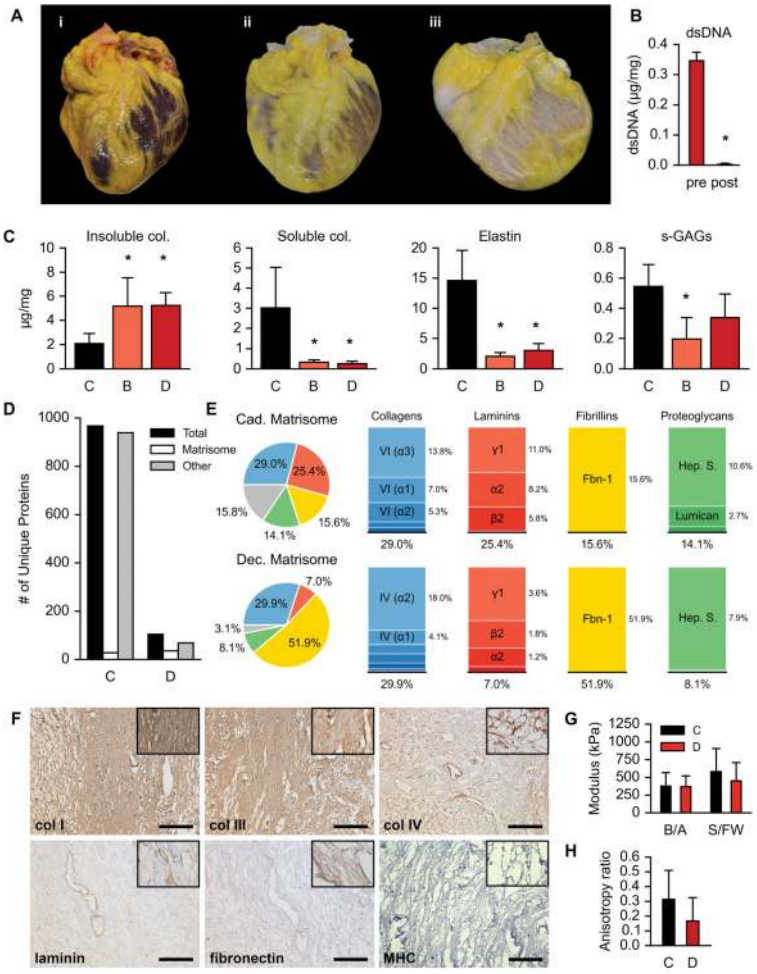

Figure 1. Biological and mechanical characterization of decellularized human myocardium

A. A human heart before (i), during (ii), and after (iii) pressure-controlled perfusion decellularization.

B. DNA content of decellularized myocardium pre- and post-perfusion with nuclease (n = 3 hearts). Normalized to tissue wet weight. Error bars are standard deviation. Asterisk (*) indicates $p < 0.05$ compared to pre-perfusion with nuclease.

C. Biochemical analysis for insoluble collagen (hydroxyproline), soluble collagen, α-elastin, and sulfated glycosaminoglycans (s-GAGs) on normal cadaveric human myocardium (C, n = 5 hearts), decellularized human cardiac matrix from hearts donated after brain death (B, n = 4), and decellularized human cardiac matrix from hearts donated after cardiac death (D, n = 4). Three tissue samples were analyzed per heart per component and the average of those three was used as the representative value for the component in that heart. Normalized to tissue wet weight. Error bars are standard deviation. Asterisks (*) indicate $p < 0.05$ compared to cadaveric condition.

D. Number of unique proteins identified through proteomics analysis in cadaveric (C) and decellularized (D) human myocardium. Total (black) represents all unique proteins identified. Matrisome (white) represents proteins in the total known to be part of the

extracellular matrix and/or basement membrane. Other (grey) represents non-matrisome proteins in the total.

E. Left: Pie charts of major components (collagens, laminins, fibrillins, and proteoglycans) in the cadaveric and decellularized matrisome based on normalized relative abundance. Right: Stacked bar charts illustrating further breakdown of the major components into specific identified proteins.

F. Immunohistochemical staining of decellularized human myocardium for collagens I, III, IV, laminin, fibronectin, and myosin heavy chain (MHC). Scale bar, 250 μm, except MHC, 100 μm.

G. Biaxial mechanical testing of cadaveric (C, n = 8 hearts) and decellularized (D, n = 10 hearts) human myocardium. B/A, base to apex axis. S/FW, septum to free-wall axis. Error bars are standard deviation.

H. Anisotropy observed in biaxial mechanical testing of cadaveric (C, n = 8 hearts) and decellularized (D, n = 10) human myocardium. Error bars are standard deviation.

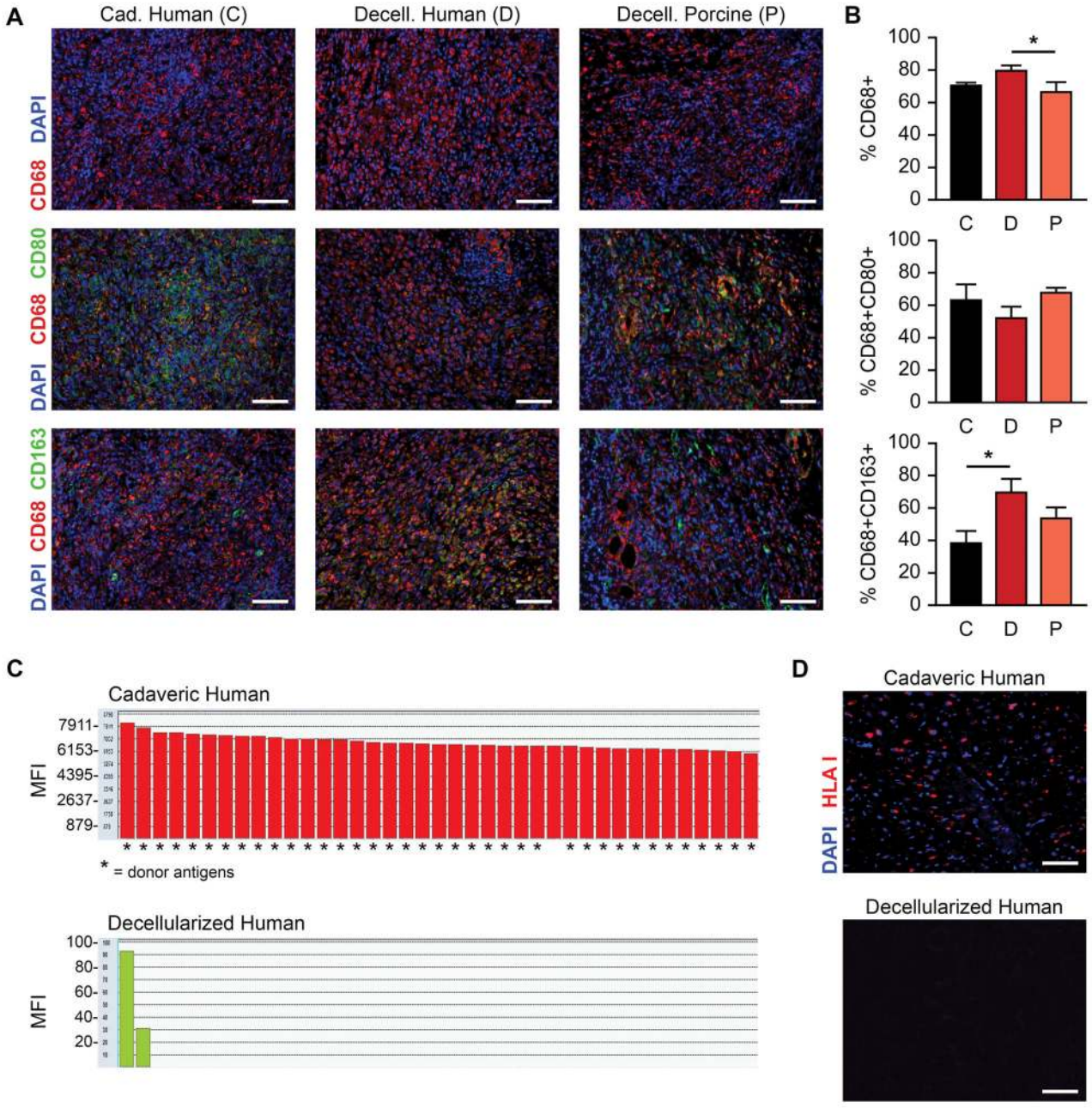

Figure 2. Immunological characterization of decellularized myocardium

A. Staining of macrophage markers CD68, CD80, and CD163 in human cadaveric (C), human decellularized (D), and porcine decellularized (P) myocardium tissue samples after two weeks implantation in a rat model. Scale bars, 100 μm.

B. Quantification of CD68+, CD68+/CD80+, and CD68+/CD163+ cells in human cadaveric (C, n = 3), human decellularized (D, n = 3), and porcine decellularized (P, n = 3) explants as a percentage of total identified cells in the field (3–5 fields averaged per explant) after two weeks implantation in a rat model. Error bars are standard deviation. Asterisk (*) indicates $p < 0.05$ between groups using an ANOVA with Tukey's post-hoc test.

C. HLA single antigen bead reactivity of implanted decellularized (i) and cadaveric (ii) human matrix, with mean fluorescence intensity (MFI) plotted against beads with specific HLA alleles (generated using HLA Fusion software, version 3.0). Asterisks (*) indicate beads presenting donor-specific antigens. MFI values annotated for increased readability. D. Immunofluorescence detection of HLA in cadaveric and decellularized human myocardium. Scale bar, 100 μm.

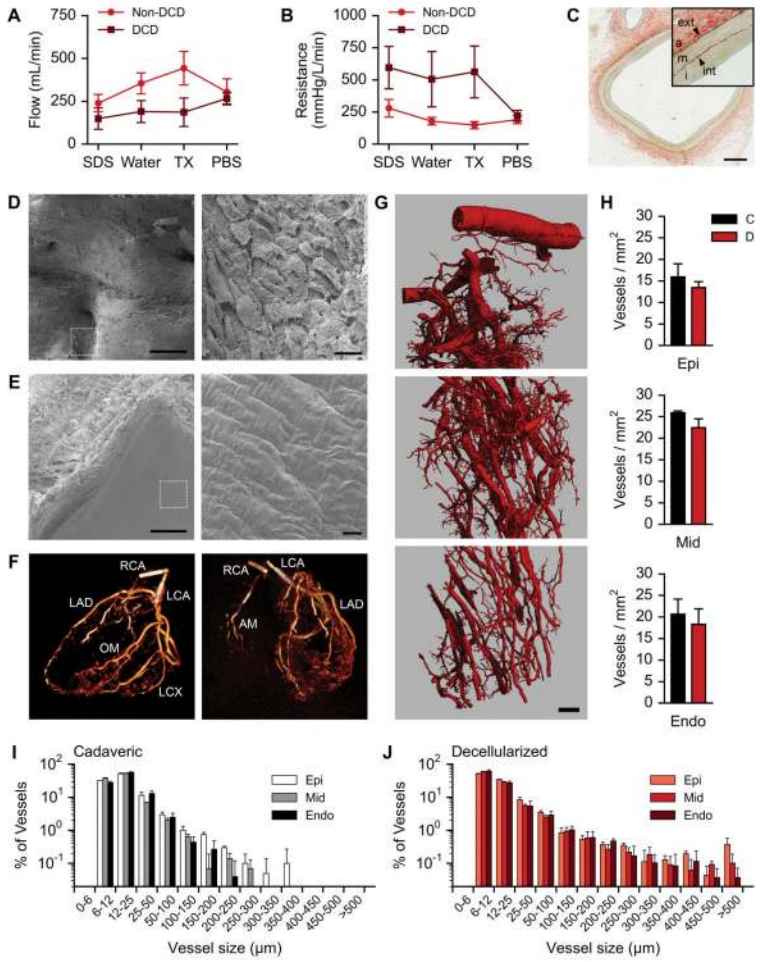

Figure 3. Characterization of vasculature in decellularized human myocardium

A. Mean flow rates of each solution under constant pressure perfusion for non-DCD (n = 3 hearts) and DCD (n = 4) populations. Error bars are SEM.

B. Mean vascular resistance calculated under constant pressure perfusion for non-DCD (n = 3 hearts) and DCD (n = 4) populations. Error bars are SEM.

C. Pentachrome staining of decellularized LAD coronary artery. Adventitia (a), tunica media (m), tunica intima (i), exterior elastic lamina (ext), interior elastic lamina (int). Scale bar, 500 μm. Color indications: elastic fibers – black, collagen – yellow, fibrin – red, mucins – blue to green.

D. Scanning electron micrograph of cadaveric LAD coronary artery. Dotted white square indicates region of higher magnification. Scale bar, 500 μm (left) and 20 μm (right).

E. Scanning electron micrograph of decellularized LAD coronary artery. Dotted white square indicates region of higher magnification. Scale bar, 500 μm (left) and 20 μm (right).

F. Cardiac CT of a decellularized human heart. Left panel: long axis view. Right panel: posterior view. LCA, left coronary artery. LAD, left anterior descending coronary artery. OM, obtuse marginal coronary artery. LCX, left circumflex coronary artery. RCA, right coronary artery. AM: acute marginal coronary artery.

G. Three-dimensional reconstruction of microvasculature in a left ventricular segment of decellularized human heart. Scale bar, 1 mm.

H. Vessel density in epicardium, mid-myocardium, and endocardium of cadaveric (C, n = 3) and decellularized (D, n = 7) heart samples.

I. Distribution of vessel sizes in the epicardium, mid-myocardium, and endocardium of cadaveric human heart samples (n = 3).

J. Distribution of vessel sizes in the epicardium, mid-myocardium, and endocardium of decellularized human heart samples (n = 7).

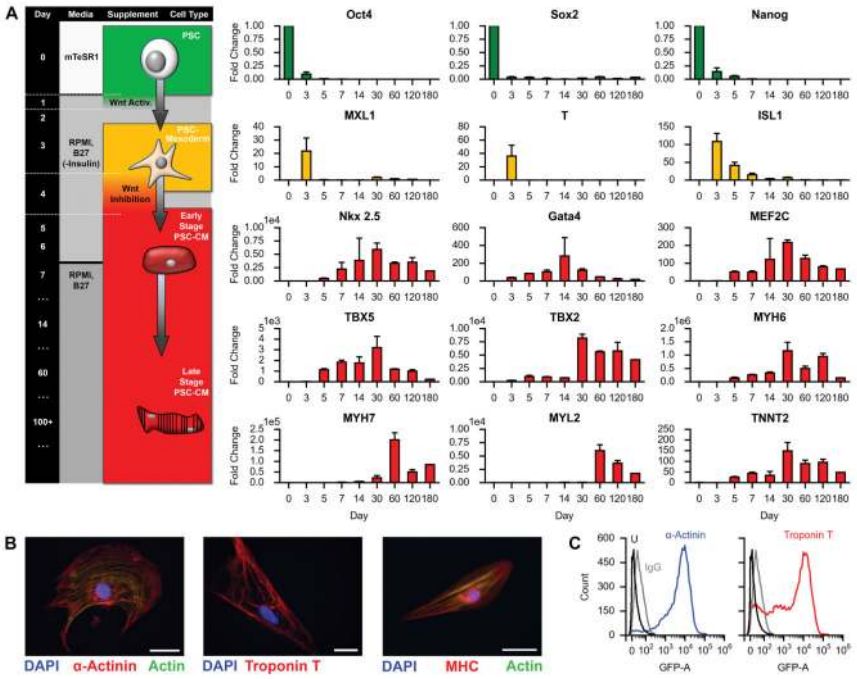

Figure 4. Generation of human iPS-derived cardiac myocytes

A. Timeline of human iPSC differentiation into late stage cardiac myocytes (days 0, 3, 5, 7, 14, 30, 60, 120, and 180) with corresponding gene activation as measured by PCR (n = 3). Error bars are standard deviation. Flow chart relates culture time with media, supplement, and cell type.

B. Immunofluorescence staining on differentiated cells isolated between days 30–60 for cardiac markers α-actinin, troponin T, and myosin heavy chain (MHC). Scale bars, 50 μm.

C. Flow cytometry analysis of a representative culture of human iPS-derived cardiac myocytes positive for α-actinin (left) and troponin T (right), isolated between days 30–60 post-differentiation.

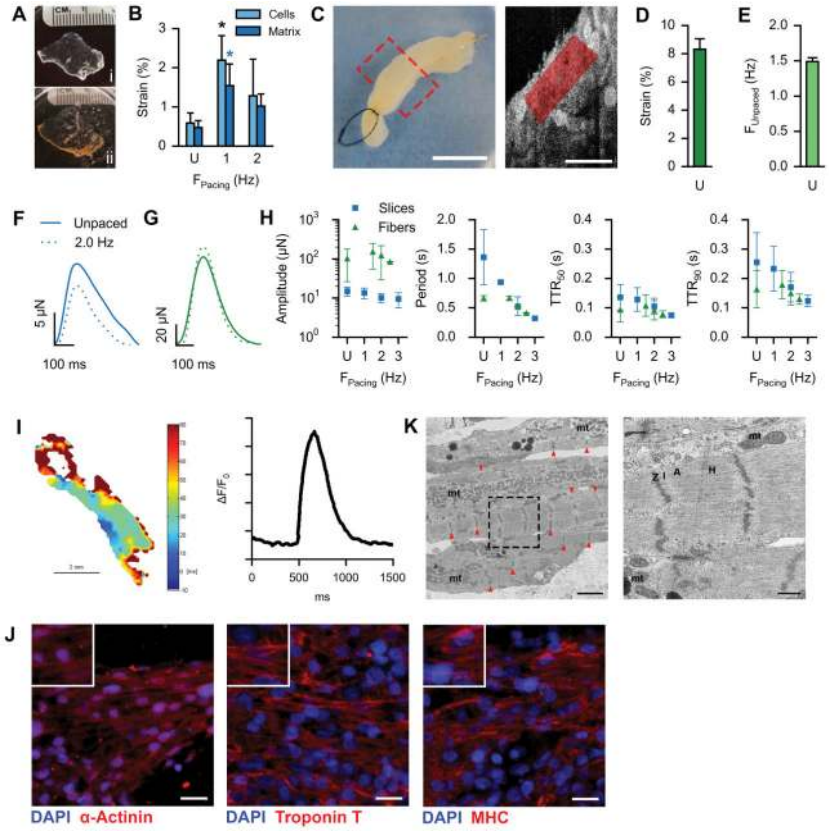

Figure 5. Generation of functional tissue constructs based on decellularized human myocardium

A. Cardiac matrix slices: decellularized human cardiac matrix slice (200 μm) in a culture well (i), seeded with iPS-derived cardiac myocytes (ii) for 120-day culture. Ruler ticks are 1 mm.

B. Area strain of matrix-seeded iPS-derived cardiac myocytes and underlying cardiac matrix, comparing spontaneous contraction (U, n = 5 beating areas) with electrical stimulation at 1 Hz (n = 4) and 2 Hz (n = 4). Error bars are standard deviation. Black and blue asterisks (*) indicate $p < 0.05$ compared to unstimulated cells and matrix, respectively.

C. Left: Macro image of a reseeded cardiac fiber. Scale bar, 5 mm. Right: Representative μOCT still-frame, depicting a longitudinal cross-section within a reseeded cardiac fiber. Red shading indicates example HDM region of interest. Scale bar, 100 μm.

D. HDM computed area strain under unpaced conditions (n = 4 fibers). Error bar indicates standard deviation.

E. HDM-captured frequencies under unpaced conditions (n = 4 fibers). Error bar indicates standard deviation.

F. Representative force curves of a single contractile area within a myocardial slice, depicting force modulation under unpaced (solid line) or paced conditions (dashed line).

G. Representative force curves of a single reseeded cardiac fiber, depicting force modulation under unpaced (solid line) or paced conditions (dashed line).

H. Mean amplitudes, periods, times to 50% relaxation (TTR_{50}), and times to 90% relaxation (TTR_{90}) of captured force-curves of slices (gray squares; n = 9, 9, 9, & 3 for unpaced, 1 Hz, 2 Hz, and 3 Hz respectively) and fibers (red triangles; n = 4, 3, 4, & 2 for unpaced, 1.5 Hz, 2

Hz, and 2.5 Hz respectively) under paced and unpaced (U) conditions. Error bars are standard deviation.

I. Conductivity map (left) and example action potential (right) from a reseeded cardiac fiber.

J. Immunofluorescence staining on reseeded cardiac fibers for cardiac markers α-actinin, troponin T, and myosin heavy chain (MHC). Scale bars, 25 μm.

K. Transmission electron micrographs of recellularized cardiac fibers. Dashed black box indicates region of higher magnification. Left panel: red arrows indicate Z-bands, mt indicates regions of mitochondria. Right panel: Z, I, A, H, & mt indicate Z-bands, I-bands, A-bands, H-bands, and mitochondria respectively. Scale bars, 2 μm and 500 nm for left and right panels respectively.

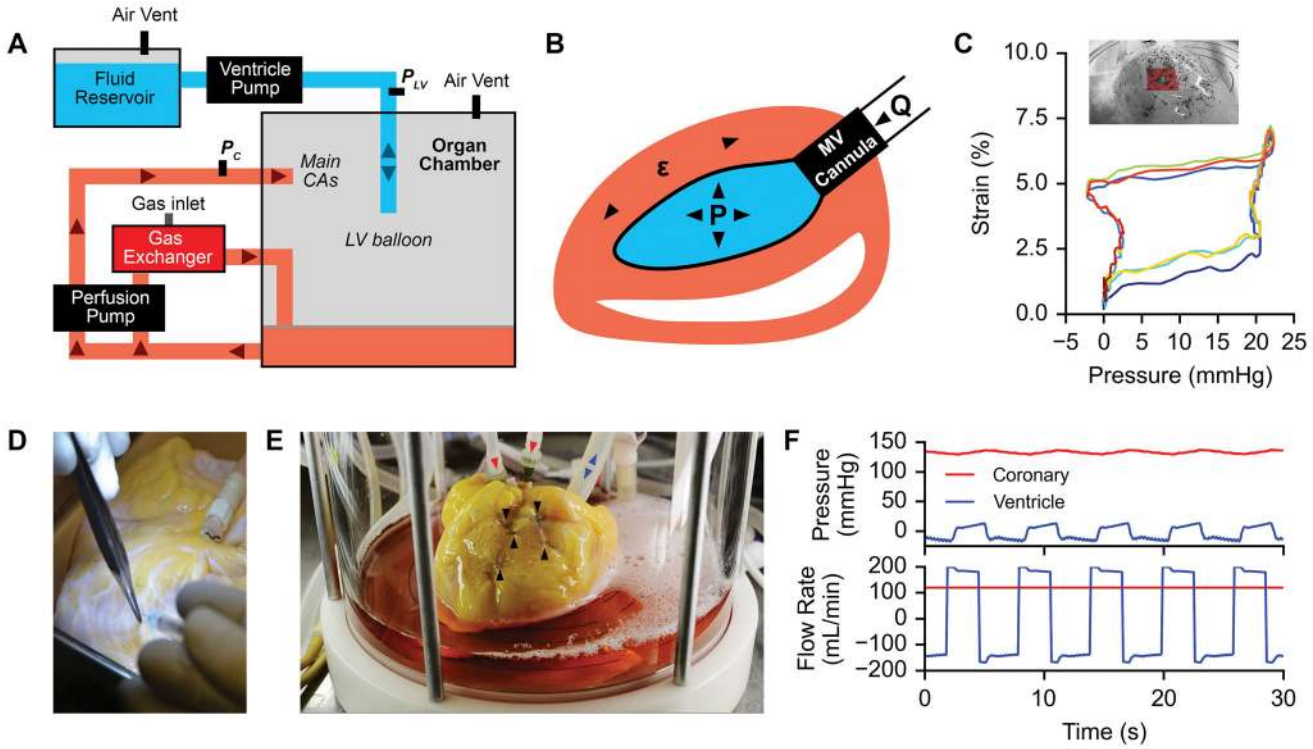

Figure 6. Human heart bioreactor

A. Schematic layout of the human heart bioreactor. Arrows indicate fluid flow directions.

B. Diagram of mechanical stimulation in the human heart bioreactor. μ, strain; P, pressure; Q, volumetric flow; MV, mitral valve.

C. Representative LV-pressure vs. matrix strain curve during mechanical stimulation in the human heart bioreactor (3 cycles plotted, starting with blue and ending with red), determined by HDM analysis on the epicardial surface of the heart (inset) through biomimetic cardiac cycles.

D. Recellularization of human acellular cardiac scaffolds by intramyocardial injection between the left anterior descending artery and the left circumflex artery.

E. Recellularized human acellular cardiac scaffold inside of the bioreactor organ chamber during biomimetic culture. Black arrows indicate intramyocardial injection locations. Red arrows indicate media perfusion into main coronary arteries. Blue arrows indicate fluid flow into left ventricle balloon during mechanical stimulation.

F. Example pressure (top) and flow rate (bottom) traces in the coronary arteries (red) and left ventricle (blue) during mechanical stimulation in the human heart bioreactor.

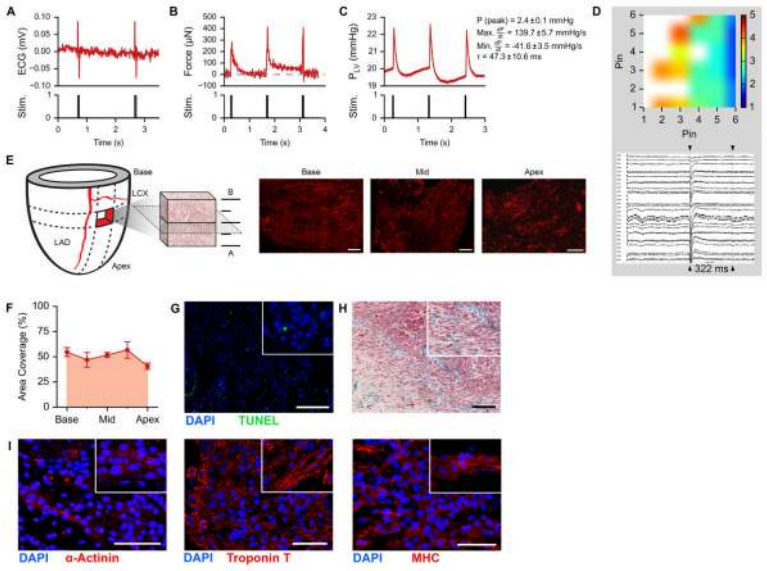

Figure 7. Repopulation of decellularized human myocardium in whole hearts with human iPS-derived cardiac myocytes

A. Electrocardiogram of a recellularized acellular cardiac scaffold during electrical stimulation (pacing).

B. Force trace of recellularized myocardium under electrical stimulation at 0.8 Hz.

C. Left ventricular pressure development in a recellularized human acellular cardiac scaffold under electrical stimulation at 0.8 Hz including corresponding mean ± SD peak pressure (P), max dP/dt, min dP/dt, and tau (n = 6 pressure pulses).

D. Conductivity map (top) and action potentials (bottom) taken from the epicardial surface of a reseeded human heart. Heat map legend labels indicate millisecond intervals.

E. Schematic of seeding volume estimation based on myosin heavy chain (MHC, red) staining images. Scale bar, 2 mm. LAD, left anterior descending coronary artery. LCX, left circumflex artery.

F. Cell coverage from base to apex of recellularized human cardiac scaffolds. Error bars are standard deviation of measurements taken from 2 adjacent tissue sections.

G. Fluorescent TUNEL of recellularized human cardiac scaffolds. Scale bar, 200 μm.

H. Trichrome staining of recellularized human cardiac scaffolds. Scale bar, 200 μm.

I. Immunofluorescent staining on recellularized human myocardium for cardiac markers α-actinin, troponin T, and myosin heavy chain (MHC). Scale bars, 50 μm.

TABLE 1

Metabolic measurements during whole-heart culture.

Measurement	Units	*Baseline*		*48-hr Media Changes*		p-value
		Mean	SD	Mean	SD	
pH	-	7.32	0.08	7.26	0.05	0.3895
pCO2	mmHg	30.00	7.26	31.75	4.85	0.7397
pO2	mmHg	164.33	22.28	187.75	38.53	0.3600
HCO3	mmol/L	15.10	0.90	14.13	0.32	0.1941
TCO2	mmol/L	16.00	1.00	15.25	0.50	0.3257
sO2%	%	99.00	0.00	99.25	0.50	0.3910
Lac	mmol/L	0.00	0.00	2.44	0.19	0.0001
Glu	mg/dL	186.33	1.53	155.75	6.70	0.0018